Chemical, Petroleum and Environmental Engineering

Preparation and Characterization of Plaster Kiln Dust-Fe₃O₄ Magnetic Nanoparticles

Dheyaa Mudher Zwayen *
Researcher

DheyaaZwayen@outlook.com

Hussein Yousif Alhussainy
Professor
College of Environmental Engineering-
University of Baghdad
Hussain_yousif2001@yahoo.com

ABSTRACT

Magnetic plaster kiln dust (MPKD) was synthesized as a unique, low-cost composite reused of byproduct plaster kiln dust (PKD), which is considered a source of air pollution. The FESEM, EDS, XRD, FTIR, VSM, and BET tests were used to characterize the MPKD. The characterization revealed that the MPKD was nanotubes non-agglomerated and super-paramagnetic with a high specific surface area (102.7 m^2/g). Compared with the specific area of other materials (composites), the MPKD could be considered a promising substance in the field of water/wastewater treatment.

Keywords: Fe₃O₄, plaster kiln dust, nanoparticles, magnetic plaster kiln dust, and nanocomposite.

تحضير وتوصيف مركب جديد من اغبارافران الجص – الجسيمات المغناطيسية النانوية Fe₃O₄

حسين يوسف الحسيني
استاذ دكتور
كلية الهندسة البيئية – جامعة بغداد

ضياء مضر زوين
باحث

الخلاصة

صُنع غبار فرن الجص المغناطيسي (MPKD) باعتباره مركب جديد منخفض التكلفة معاد استخدامه من المنتج الثانوي غبار فرن الجص (PKD) الذي يعد مصدرا لتلوث الهواء. استخدمت اختبارات FESEM، EDS، XRD، FTIR، VSM و BET لتوصيف MPKD. كشف التوصيف أن MPKD كانت عبارة عن أنابيب نانوية غير مكتلة و فائقة المغناطيسية ذات مساحة سطحية عالية (102.7 م2/ جم). بالمقارنة مع مساحات المواد الخرى (مركبات)، ممكن اعتبار MPKD مادة واعدة في مجال معالجة المياه/ المخلفات السائلة.

الكلمات الرئيسية: Fe₃O₄، غبار فرن الجص، الجسيمات النانوية، غبار فرن الجص المغناطيسي، و مركب نانوي.

1. INTRODUCTION

With the rapid development of nanotechnology in recent years, considerable attention to synthesizing various types of magnetic nanoparticles was conducted to find a solution of environmental issues like adsorption of dyes by magnetic halloysite (**Bonetto et al., 2015**), remediation of contaminated soils and oils pill (**Nnaji, 2017**), removing radionuclide (**Zhang and Liu, 2020**), adsorbing contaminants from aqueous or gaseous effluents (**Boparai et al., 2011**), and accelerating the coagulation of sewage (**Popowich et al., 2015**). The unique properties of nanomaterials have been employed for several uses, especially in medicine such as diagnostic purposes (**Baetke et al., 2015**), optical and electronic devices application (**Nguyen, 2014**), catalysis such as catalysis of gold nanoparticles deposited on metal oxides (**Haruta, 2002**), ceramics for applications in drug delivery (**C Thomas, et al., 2015**), and magnetic data storage (**Gubin et al., 2002**). Ostensibly, the advantages of magnetic nanoparticles are high magnetic properties, a high number of surface-active sites, and large surface area resulting in increased uptake (high removal rate of contaminants) and easy, rapid separation of adsorbent from solution by the magnetic field. Then, the harmful components can be removed from the magnetic particles then can be reused. Several essential aspects have been taken into account in improving the physical and chemical properties of the materials by controlling the chemical composition, size, shape, and morphology (**Panneerselvam et al., 2013; Abdullah et al., 2017).**

Iron oxide, among magnetic nanoparticles, has gained wide attention. These nanoparticles are super-paramagnetic at room temperature, low toxicity, and producing no contaminants (**Dung et al., 2009; Jiang et al., 2014).**

Many researchers in recent years prepared and characterized composites from magnetic nanoparticles and low-cost materials such as tea waste (**Panneerselvam et al., 2011**), attapulgite (**Zhou et al., 2011**), zeolite (**Salem Attia et al., 2014; Mohammed, 2019**), montmorillonite (**Chang et al., 2016**), and bentonite (**Abd Ali, 2015; Mohammed and Samaka, 2018**).

Plaster kiln dust is solid and white powdered matter extracted and collected from the large gas emission through smoke chimney or smokestacks that are found at the ending of the plaster kiln (or gypsum kiln) production facility. The sources of emissions in plaster (gypsum) kiln plants are often controlled through fabric filters and electrostatic precipitators as exhibited. Gypsum is considerd the source material for plaster (Juss) industries, and it is used as a retarder in the cement industry. Gypsum ($CaSO_4 . 2H_2O$) is the calcium sulfate dihydrate, a gray or white natural mineral occurrence. The gypsum must be dehydrated partly, to produce plaster, or calcined to manufacture calcium sulfate half hydrate ($CaSO_4 . \frac{1}{2}H_2O$), usually calling stucco. In most plants, the calcination to produce stucco takes place in roughly 250 to 300 °F (120 to 150 °C), at that 1 ton of gypsum calcines to about 0.85 ton of stucco, and the rest is emissions as particulate matter disposal of the byproduct from gypsum plants is frequently the biggest problem. In Europe, the byproduct gypsum method of disposal includes discharge into the sea or estuaries, dumping on land, and dumping in the excavated area and old mines (**Organization for Economic Co-operation and Development, 1977; US EPA, 1997; Jassim, 2019; US EPA, 1997; El-Fadel et al., 2009; the Ministry of Environment, 1994**). From the environmental viewpoint, the PKD adversely effects the ecosystem. Industrial emissions are associated with risks to human health and the natural environment (** El-Fadel, 2009; Alrawashdeh et al., 2014).**

The present study aims to prepare and characterize composite from byproduct low-cost plaster kiln dust (PKD) and magnetic nanoparticles Fe_3O_4.

2. MATERIALS AND METHODS

Composite Preparation and Characterization

The byproduct PKD, **Fig. 1 (a)** was collected from local factories located in Iraq (the Modern Investment Mechanical Plaster Factory). The PKD was coated by the Fe_3O_4 magnetic nanoparticles (Merck USA; 10-20 nm in diameter) to produce magnetic plaster kiln dust (MPKD) through the wet impregnation method represented in **(Makarchuk, et al., 2016; Daneshfozoun, et al., 2017)**. The Fe_3O_4, magnetic nanoparticles powder, **Fig. 1 (b),** was scattered and sonicated in deionized water for 3 min using sonication (1200W Ultrasonic Homogenizing and Mixing Liquid Chemicals - MSK-USP-12N). Then the PKD was added to the magnetic fluid to achieve a percent of Fe_3O_4 to PKD as (20 %). The new mixture was sonicated again for 10 min and stirred for one hour using a magnetic stirrer (SH-3) to adsorb magnetite onto the PKD. The synthesized adsorbent (MPKD) was separated by an external magnetic field and dried at 100 °C for one day and then milled for 60 min at a speed of 500 rpm, and the final composite was shown in **Fig. 1 (c)**.

(a)   (b)   (c)
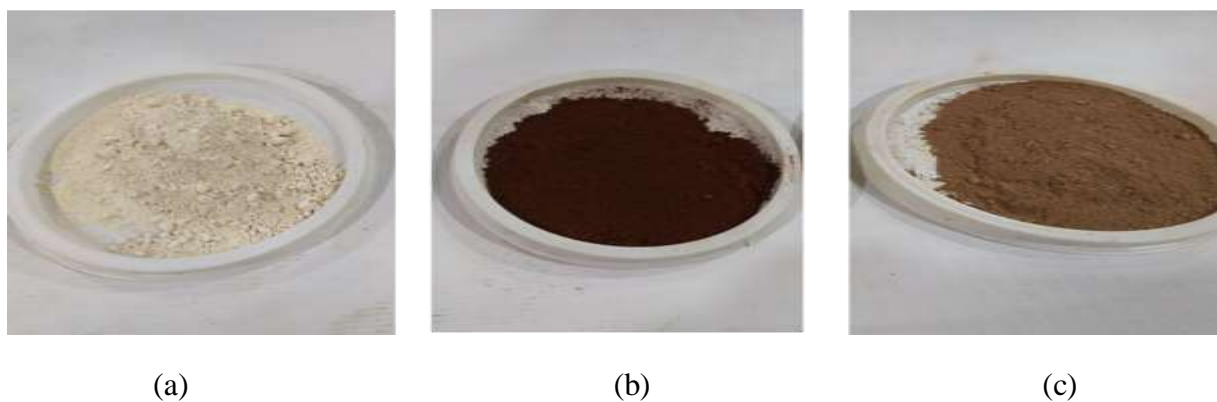
Figure 1. a. PKD, b. Fe3O4, c. MPKD.

The characterization study of the PKD and MPKD included a description of morphology, shape, and size before and after coating to explore changes in surface topology via field emission scanning electron microscope (FESEM MIRA3 TESCAN, HV: 10 kV). Elemental analysis for the above materials performed by energy dispersive spectroscopy (EDS) operated at an accelerating voltage of 10 kV.

The metal structure of both PKD and MPKD was detected by X-ray diffraction (XRD, Phillips Xpert) at room temperature with CuKα radiation source (λ= 0.154 nm wavelength) generated at 40 kV/40 mA. The functional group of the above materials was also examined using Fourier transform infrared spectroscopy (FTIR, Shimadzu) by mixing samples with KBr at a 1:1 ratio.

Physical properties such as specific surface area and pore size distribution were calculated by the Brunauer–Emmett–Teller (BET) model and the Barrett–Joyner–Halenda (BJH) method, respectively.

The magnetization of samples was carried out using a vibrating sample magnetometer (VSM, EZ7 model Microsense) at room temperature. The sample was put in a uniform magnetic field to analyze the magnetic properties.

3. RESULTS AND DISCUSSION
3.1. Characterization
3.1.1. FESEM and EDS

The FESEM analysis was shown in **Fig. 1** with different scales. The appearance of the PKD particles was agglomerated nanotubes crystal with an average diameter of 53 nm of different sizes, as shown in **Fig. 1 (a)** and **(b)**. The surface of PKD was highly porous textural with cracks and fissures (dark parts). These configurations increased the possibility of the Fe_3O_4 nanoparticles to adhere to the PKD particle's surface. After the coating process, the cracks on the surface of PKD particles disappeared and covered by the Fe_3O_4 nanoparticles that appeared as a bright spot, as shown in **Fig. 1 (c)** and **(d)**. Also, the agglomeration of nanotubes no longer existed. Besides, new cavities were formed. Thus, the coating of PKD to produce MPKD was successful.

Another verification of the coating was achieved by the EDS spectrum, as shown in **Fig. 2**. The presence of the Fe_3O_4 nanoparticles onto the PKD particle surface appeared in new peaks of the iron element (Fe) and represented by a percent of 2.81 % in **Fig. 2 (b)**.

(a)

(b)

(c)

(d)
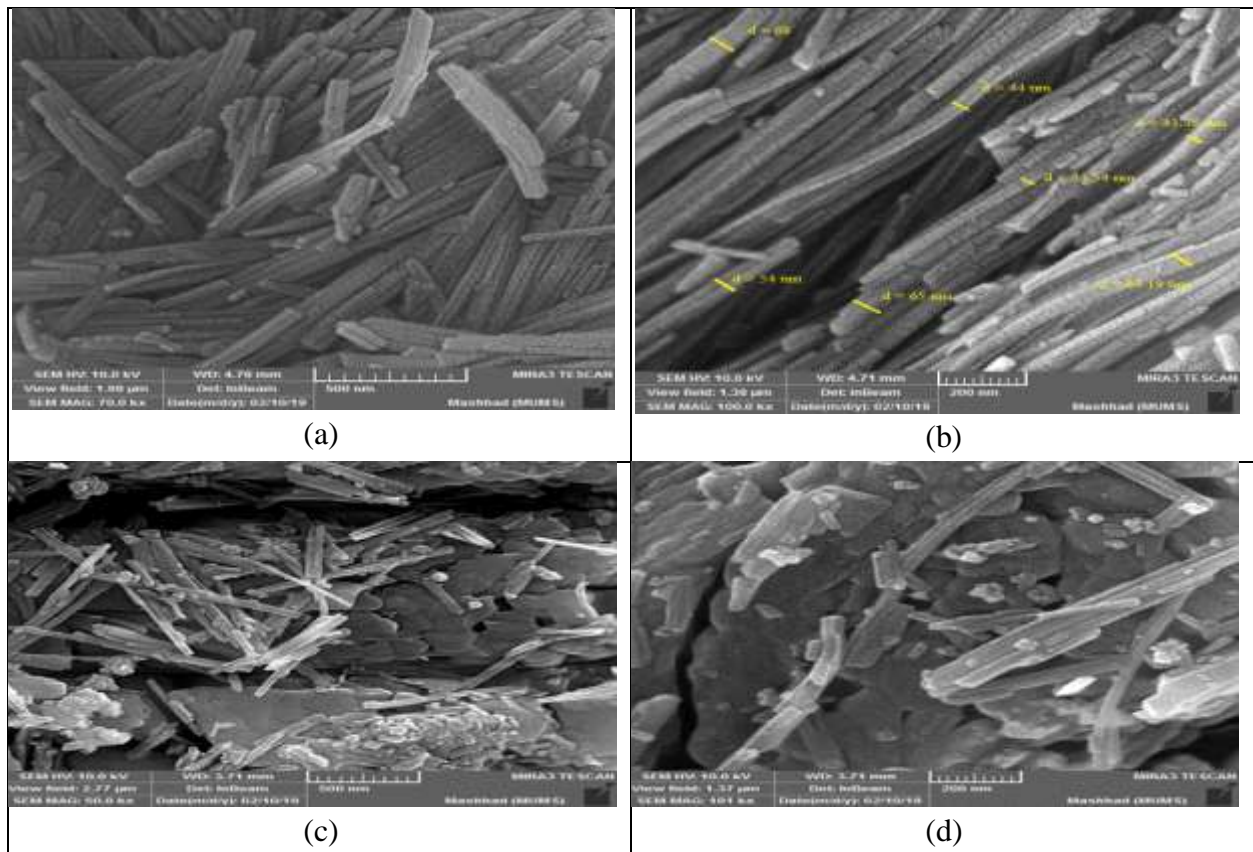
Figure 1. a and b. The FESEM images for PKD.
c and d. The FESEM images for MPKD.
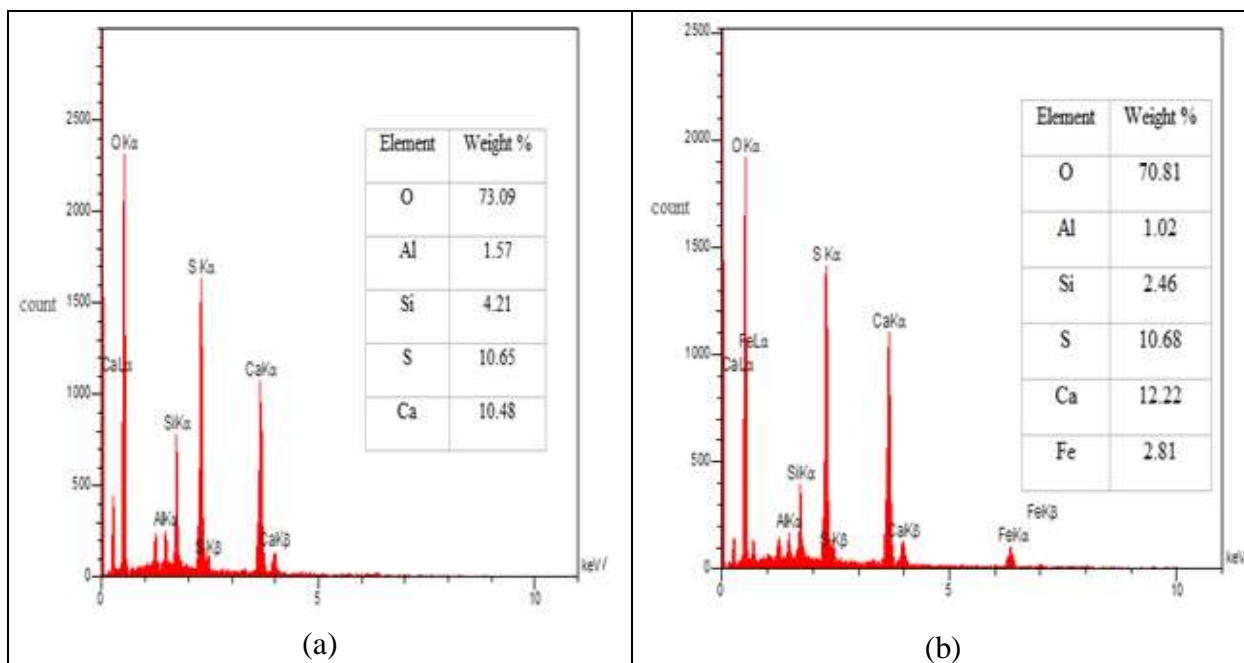
Figure 2. a. The EDS spectrum of the PKD, b. The EDS spectrum of the MPKD.

3.1.2. XRD and FTIR analysis

The XRD patterns (according to the International Centre for Diffraction Data, ICDD) of the PKD and MPKD were exhibited in **Fig. 3**. Based on the XRD analysis of the PKD, the noticeable peaks referred to several compounds of gypsum (the main constituent), quartz, calcium carbonate, and calcium sulfate. After coating, new diffraction peaks at 2Θ= 29.76º, 35.98º, 36.64º, 42.35º, 43.36º, 47.82º, 54.17º, 63.07º and 72.85º could be identified as magnetite (Fe_3O_4). These results referred that the magnetic nanoparticles successfully adhered to the surface of the PKD.

FTIR spectra for PKD and MPKD were scanned in the range of 4000- 400 cm^{-1}, as shown in **Fig. 4 (a)** and **(b)**, respectively. From **Fig. 4 (a)**, the bands located around 3547.09, 3493.09, and 3406.29 were typically ascribed to stretching vibration O-H groups due to H_2O molecules in gypsum constituent. The band located at 3246.2 cm^{-1} was attributed to N-H stretching. The bands around 1799.59 cm^{-1} were imputed to C-H bending. The band around 1683.86 cm^{-1} was due to C=N stretching. The trough at 1622.13 cm^{-1} was seen for C=C stretching. The peak observed around 1433.11 and 1369.46 cm^{-1} corresponded to C-H bending. The bands located at 1138 cm^{-1} and 1118.71 were typically attributed to C-O stretching. The band around 1039.63 cm^{-1} was due to S=O stretching. The peak at 987.55 cm^{-1} was assigned to C=C bending. Carboxylic acids (general formula R–COOH) was indicated by a peak of 875.68 cm^{-1} **(Socrates, 2004).** The presence of silica in this sample was observed by 785.03 cm^{-1}. The band at 704.02 cm^{-1} was attributed to the C-C stretching absorptions. The peaks at 669.3 and 601.79 cm^{-1} were assigned to the stretching and bending modes of sulfate of the gypsum spectrum. Compared with the FTIR of the PKD, variations in the percentage of transmittance (T%) values of several peaks in the MPKD spectra were obvious. The new peaks at 599.86 and 507.28 cm^{-1} were indicated to the Fe-O

stretching vibration group, which successfully coated the PKD (**Soliman et al., 2016**). Furthermore, the shifting of most absorption peaks and the emergence of new peaks with the disappearance of others were related to the coating process and verified the binding of iron oxide onto the PKD.
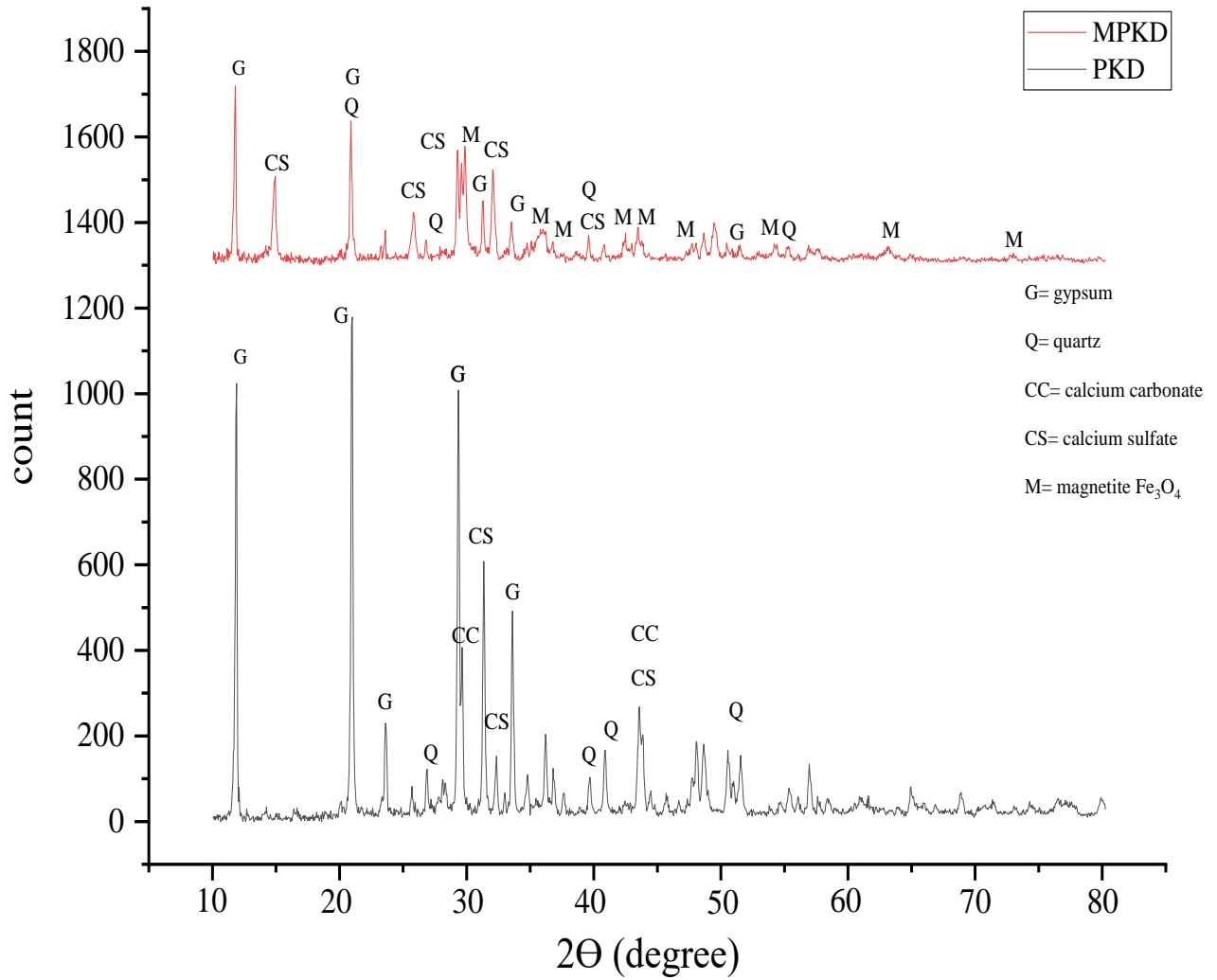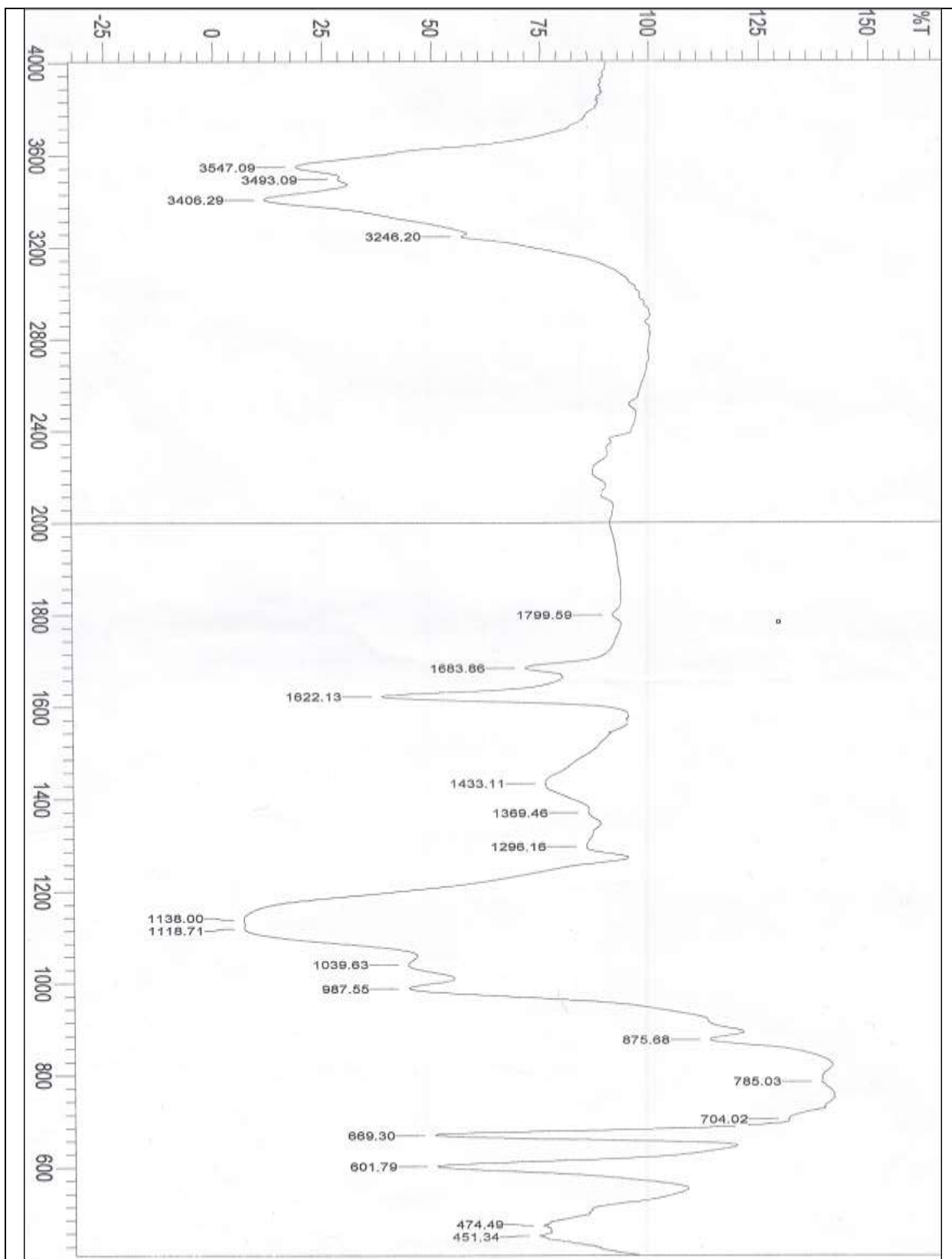

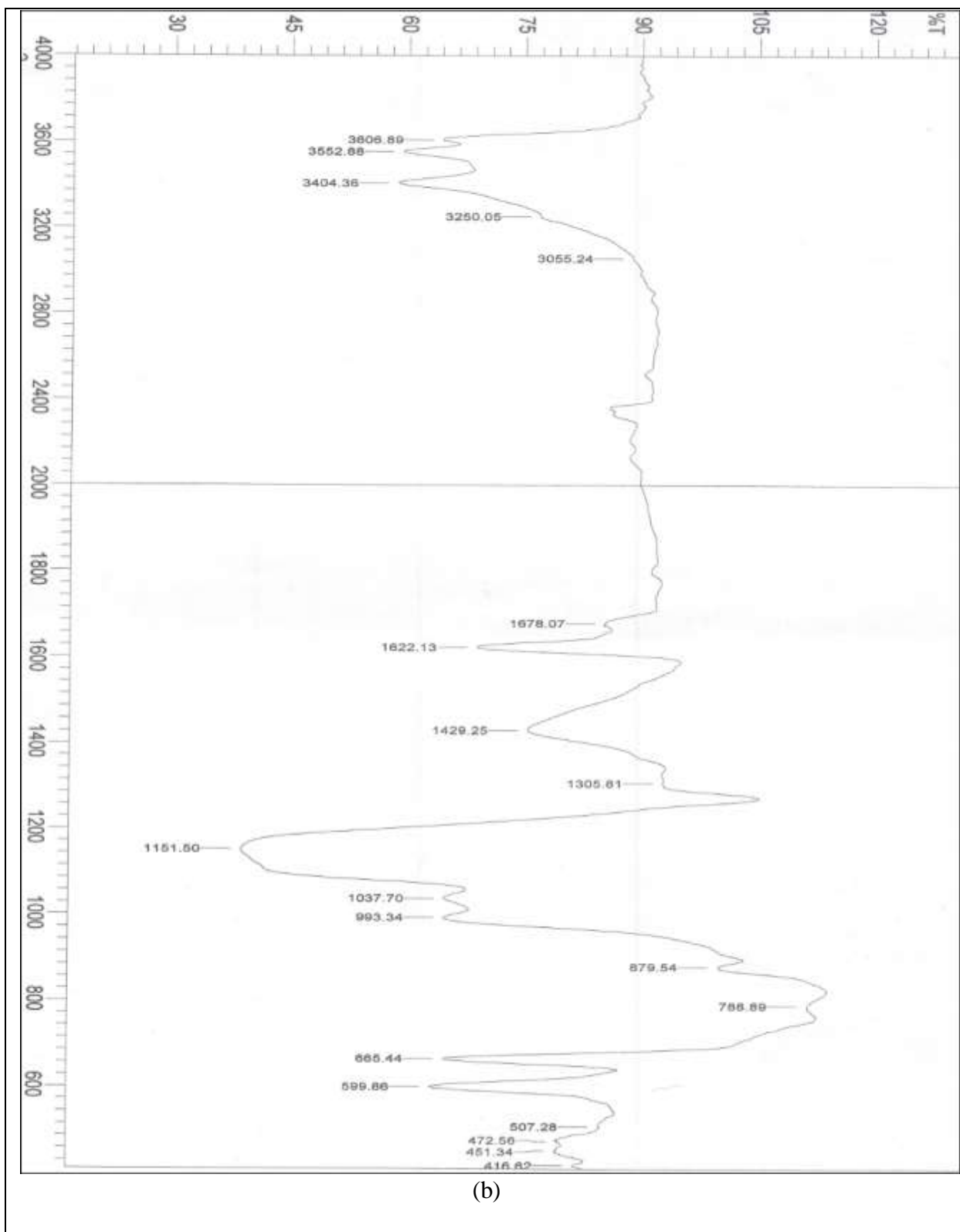**Figure 3.** The XRD patterns of the PKD and MPKD.

(a)

(b)

Figure 4. a. The FTIR spectra of the PKD, b. The FTIR spectra of the MPKD.

.

3.1.3.   Magnetic properties

Magnetometry (by field -7.02≤H≤7.02 kOe) of the MPKD was represented as a hysteresis loop and displayed in **Fig. 5**. The results indicated that this material was a soft magnet or super-paramagnetic due to the value of remanence (M_r) and coercivity (H_c) closed to zero. The saturation magnetization was 29.12 emu/g, so the MPKD possessed a good response to an external magnetic field. Similar results were found by **(Hu, et al., 2014).**
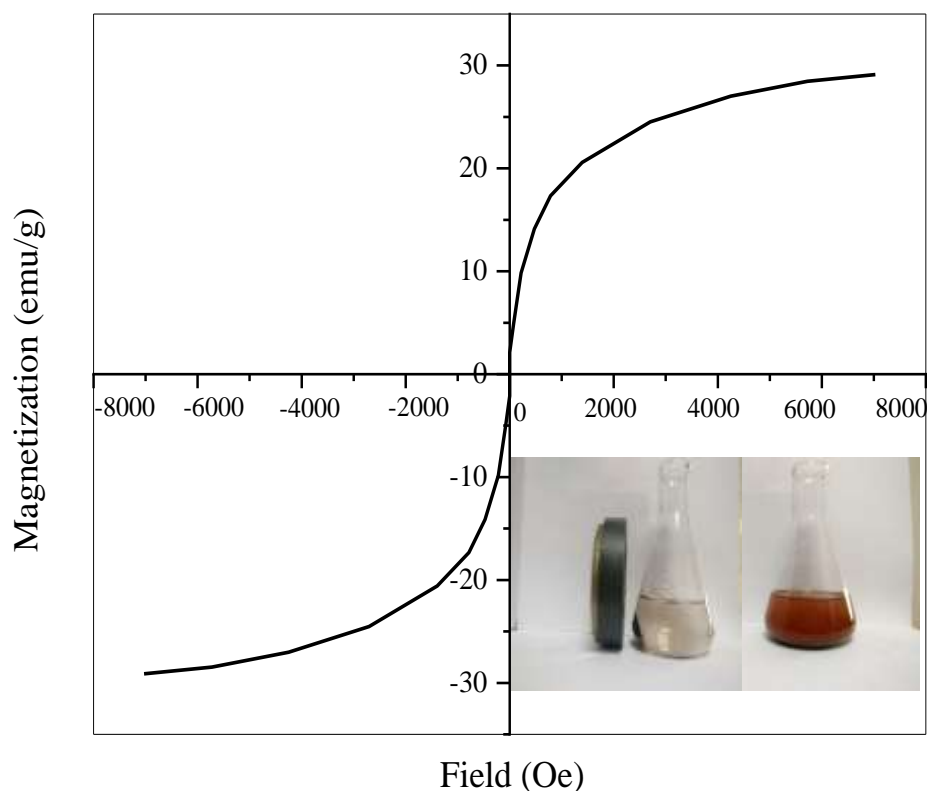
Figure 5. Magnetization curve of the MPKD.

3.1.4.   BET analysis

The BET analysis of PKD, MPKD, and Fe_3O_4 was determined and reported in **Table 1**. As a whole, the area of particles surface and entire pores volume of the MPKD were greater than any of the PKD and Fe_3O_4 as many researchers like **(Orolínová and Mockovčiaková, 2009; Yan et al., 2016)** who discovered the same results after coating the raw materials by iron oxide, which can provide more effective sites for the uptake of pollutants. This can be described by the growth (development) of the micropores and mesopores composition with the creation of a magnetite layer of nanosized on the pore's surfaces of the PKD, as verified by FESEM in **Fig. 1b**, where new cavities and pores and appear after coating. The PKD and MPKD have an average pore diameter, which shows that both materials are mesoporous (between 2 and 50 nm). The data of **Table 1**

clearly indicate that the Fe_3O_4 magnetic nanoparticles easily agglomerate together. Therefore, the more Fe_3O_4 nanoparticles, the smaller the BET values. These results were in a good consensus with some publications **(Chang, et al., 2016; Lou et al., 2015; Hashemian et al., 2015).**

Table 1. The BET results.

Characteristic	Fe_3O_4	PKD	MPKD
BET surface area (m^2/g)	85	46.7	102.7
Total pore volume (cm^3/g)	-	0.113	0.308
BJH average pore diameter (nm)	-	9.2	15.4

4. CONCLUSIONS

The byproduct PKD was coated by magnetic nanoparticles Fe_3O_4, and the new composite (MPKD) characterized by many tests. The morphology and the elemental structure proved successful development of the MPKD; besides, it acquired higher surface area (by double) with new effective functional groups as verification by the FTIR test. Preparation and characterization of the MPKD were not mentioned previously, as shown in the literature survey. So, it could be considered as an efficient composite compared to other publications in **Table 2**.

Table 2. Comparison of the surface area of the different materials before and after coating by magnetic nanoparticles.

Material	Surface area (m^2/g)	Reference
Attapulgite	29.34	**(Liu et al., 2008)**
Fe_3O_4/ attapulgite	98.93	**(Liu et al., 2008)**
Tea waste	22.3	**(Panneerselvam et al., 2011)**
Fe_3O_4/ tea waste	27.5	**(Panneerselvam et al., 2011)**
Bentonite	65.1	**(Yan et al., 2016)**
Fe_3O_4/ bentonite	110.7	**(Yan et al., 2016)**
Montmorillonite	187.30	**(Chang et al., 2016)**
Fe_3O_4/ montmorillonite	147.92	**(Chang et al., 2016)**
Saponite	34.64	**(Makarchuk et al., 2016)**
Fe_3O_4/ saponite	53.03	**(Makarchuk et al., 2016)**
Bentonite	62.3	**(Mohammed and Samaka, 2018)**
Fe_3O_4/ bentonite	98.55	**(Mohammed and Samaka, 2018)**
PKD	46.7	**This study**
MPKD	102.7	**This study**

REFERENCES

- Abd Ali, Z.T., 2015. A comparative Isothermal and Kinetic Study of the Adsorption of Lead (II) from Solution by Activated Carbon and Bentonite. *Journal of Engineering*, *21*(7), pp.45-58.

- Abdullah, N.H., Shameli, K., Abdullah, E.C. and Abdullah, L.C., 2017. A facile and green synthetic approach toward fabrication of starch-stabilized magnetite nanoparticles. *Chinese Chemical Letters*, *28*(7), pp.1590-1596.

- Alrawashdeh, A.I., Al-Rawajfeh, A.E., Al-Bedoor, A.A., Al-Shamaileh, E.M., and Al-Hanaktah, M.N., 2014. Production of plaster from gypsum deposits in south Jordan: improvement of the setting time. *Journal of Chemical Technology and Metallurgy*, *49*(3), pp.293-302.

- Baetke, S.C., Lammers, TGGM, and Kiessling, F., 2015. Applications of nanoparticles for diagnosis and therapy of cancer. *The British journal of radiology*, *88*(1054), p.20150207.

- Bonetto, L.R., Ferrarini, F., De Marco, C., Crespo, J.S., Guégan, R., and Giovanela, M., 2015. Removal of methyl violet 2B dye from aqueous solution using a magnetic composite as an adsorbent. *Journal of Water Process Engineering*, *6*, pp.11-20.

- Boparai, H.K., Joseph, M., and O'Carroll, D.M., 2011. Kinetics and thermodynamics of cadmium ion removal by adsorption onto nano zerovalent iron particles. *Journal of hazardous materials*, *186*(1), pp.458-465.

- C Thomas, S., Kumar Mishra, P. and Talegaonkar, S., 2015. Ceramic nanoparticles: fabrication methods and applications in drug delivery. *Current pharmaceutical design*, *21*(42), pp.6165-6188.

- Chang, J., Ma, J., Ma, Q., Zhang, D., Qiao, N., Hu, M., and Ma, H., 2016. Adsorption of methylene blue onto Fe3O4/activated montmorillonite nanocomposite. *Applied Clay Science*, *119*, pp.132-140.

- Daneshfozoun, S., Abdullah, M.A., and Abdullah, B., 2017. Preparation and characterization of magnetic biosorbent based on oil palm empty fruit bunch fibers, cellulose, and Ceiba pentandra for heavy metal ions removal. *Industrial Crops and Products*, *105*, pp.93-103.

- Dung, T.T., Danh, T.M., Hoa, L.T.M., Chien, D.M. and Duc, NH, 2009. Structural and magnetic properties of starch-coated magnetite nanoparticles. *Journal of Experimental Nanoscience*, *4*(3), pp.259-267.

- El-Fadel, M., Abi-Esber, L., and Ayash, T., 2009. Managing emissions from highly industrialized areas: Regulatory compliance under uncertainty. *Atmospheric Environment*, *43*(32), pp.5015-5026.

- Gubin, S.P., Spichkin, Y.I., Yurkov, G.Y. and Tishin, A.M., 2002. Nanomaterial for high-density magnetic data storage. *RUSSIAN JOURNAL OF INORGANIC CHEMISTRY C/C OF ZHURNAL NEORGANICHESKOI KHIMII*, *47*(SUP/1), pp.S32-S67.

- Haruta, M., 2002. Catalysis of gold nanoparticles deposited on metal oxides. *Caltech*, *6*(3), pp.102-115.

- Hashemian, S., Saffari, H., and Ragabion, S., 2015. Adsorption of cobalt (II) from aqueous solutions by Fe 3 O 4/bentonite nanocomposite. *Water, Air, & Soil Pollution*, *226*(1), p.2212.

- Jiang, L., Zhang, C., Wei, J., Tjiu, W., Pan, J., Chen, Y., and Liu, T., 2014. Surface modifications of halloysite nanotubes with super-paramagnetic Fe 3 O 4 nanoparticles and carbonaceous layers for efficient adsorption of dyes in water treatment. *Chemical Research in Chinese Universities*, *30*(6), pp.971-977.

- Liu, Y., Liu, P., Su, Z., Li, F., and Wen, F., 2008. Attapulgite–Fe3O4 magnetic nanoparticles via co-precipitation technique. *Applied Surface Science*, *255*(5), pp.2020-2025.

- Lou, Z., Zhou, Z., Zhang, W., Zhang, X., Hu, X., Liu, P., and Zhang, H., 2015. Magnetized bentonite by Fe3O4 nanoparticles treated as adsorbent for methylene blue removal from aqueous solution: Synthesis, characterization, mechanism, kinetics, and regeneration. *Journal of the Taiwan Institute of Chemical Engineers*, *49*, pp.199-205.

- Makarchuk, O.V., Dontsova, T.A., and Astrelin, I.M., 2016. Magnetic nanocomposites as efficient sorption materials for removing dyes from aqueous solutions. *Nanoscale research letters*, *11*(1), p.161.

- Mohammed, A.A., and Isra'a, S.S., 2018. Bentonite coated with magnetite Fe3O4 nanoparticles as a novel adsorbent for copper (II) ions removal from water/wastewater. *Environmental Technology & Innovation*, *10*, pp.162-174.

- Mohammed, R.R., 2019. Comparison Study of Adsorption of Lead and Methylene Blue on Zeolite, Activated Carbon and Their Composite Materials. *Journal of Engineering*, *25*(8), pp.129-148.

- Nguyen, C.V., 2014. Opto-electronic devices with nanoparticles and their assemblies.

- Nnaji, J. C., 2017. Nanomaterials for Remediation of Petroleum Contaminated Soil and Water. *Umudike Journal of Engineering and Technology, 3*(2)*, pp.23-29.

- Organization for Economic Co-operation and Development, 1977. Emission control costs in the fertilizer industry. Washington, DC.

- Panneerselvam, P., Morad, N., and Lim, Y.L., 2013. Separation of Ni (II) ions from aqueous solution onto maghemite nanoparticle (γ-Fe3O4) enriched with clay. *Separation Science and Technology*, *48*(17), pp.2670-2680.

- Popowich, A., Zhang, Q. and Le, X.C., 2015. Removal of nanoparticles by coagulation. *J. Environ. Sci*, *38*, pp.168-171.

- Salem Attia, T.M., Hu, X.L. and Yin, D.Q., 2014. Synthesized magnetic nanoparticles coated zeolite (MNCZ) for the removal of arsenic (As) from aqueous solution. *Journal of Experimental Nanoscience*, *9*(6), pp.551-560.

- Socrates, G., 2004. *Infrared and Raman characteristic group frequencies: tables and charts*. John Wiley & Sons.

- Soliman, F.M., Yang, W., Guo, H., Shinger, M.I., Idris, A.M., and Hassan, E.S., 2016. Synthesis and characterization of a high oil-absorbing poly (methyl methacrylate-butyl acrylate)/ATP-Fe3O4 magnetic composite material. *American Journal of Polymer Science and Technology*, *2*(1), pp.1-10.

- US EPA, AP-42, 1997. *Compilation of Air Pollutant Emission Factors, AP-42*, Volume 1: Stationary Point and Area Sources, 5th ed., Office of Air Quality Planning and Standards, US EPA, Research Triangle Park, NC.

- Yan, L., Li, S., Yu, H., Shan, R., Du, B., and Liu, T., 2016. Facile solvothermal synthesis of Fe3O4/bentonite for efficient removal of heavy metals from aqueous solution. *Powder Technology*, *301*, pp.632-640.

- Zhang, X. and Liu, Y., 2020. Nanomaterials for radioactive wastewater decontamination. *Environmental Science: Nano*, *7*(4), pp.1008-1040.

- Zhou, S., Xue, A., Zhao, Y., Wang, Q., Chen, Y., Li, M., and Xing, W., 2011. Competitive adsorption of Hg2+, Pb2+ and Co2+ ions on polyacrylamide/attapulgite. *Desalination*, *270*(1-3), pp.269-274.